

AD-A106 724

AKRON UNIV OH INST OF POLYMER SCIENCE

F/G 11/1

FAILURE LOADS FOR MODEL ADHESIVE JOINTS SUBJECTED TO TENSION, C--ETC(U)

OCT 81 A N GENT, O H YEON

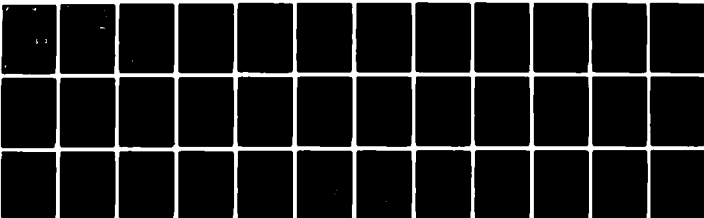
N00014-76-C-0408

UNCLASSIFIED

TR-14

NL

1 of 1
Pages



END
DATE
FILMED
1 1 81
DTIC

12

LEVEL II

AD A106724

OFFICE OF NAVAL RESEARCH
Contract N00014-76-C-0408
Project NR 092-555

Technical Report No. 14

FAILURE LOADS FOR MODEL ADHESIVE JOINTS SUBJECTED
TO TENSION, COMPRESSION OR TORSION

by

A. N. Gent and O. H. Yeoh

Institute of Polymer Science
The University of Akron
Akron, Ohio 44325

DTIC
ELECTE
NOV 3 1981
S D
B

October, 1981

Reproduction in whole or in part is permitted
for any purpose of the United States Government

Approved for Public Release; Distribution Unlimited

DTIC FILE COPY

8 1 11 02 225

REPORT DOCUMENTATION PAGE		READ INSTRUCTIONS BEFORE COMPLETING FORM
1. REPORT NUMBER Technical Report No. 14	2. GOVT ACCESSION NO. AD-A106724	3. RECIPIENT'S CATALOG NUMBER
4. TITLE (and Subtitle) (6) Failure Loads for Model Adhesive Joints Subjected to Tension, Compression or Torsion.		5. TYPE OF REPORT & PERIOD COVERED (9) Technical Report.
7. AUTHOR(s) (10) A. N. /Gent O. H. /Yeoh		6. PERFORMING ORG. REPORT NUMBER
8. PERFORMING ORGANIZATION NAME AND ADDRESS Institute of Polymer Science The University of Akron Akron, Ohio 44325 (14) TR-14		9. CONTRACT OR GRANT NUMBER(s) N00014-76-C-0408 NR 092-555
11. CONTROLLING OFFICE NAME AND ADDRESS Office of Naval Research Power Program Arlington, VA 22217 (11) 25		10. PROGRAM ELEMENT, PROJECT, TASK AREA & WORK UNIT NUMBERS NR 092-555
14. MONITORING AGENCY NAME & ADDRESS (if different from Controlling Office) (12) 42		12. REPORT DATE Oct 81
		13. NUMBER OF PAGES
		15. SECURITY CLASS. (of this report) Unclassified
		15a. DECLASSIFICATION/DOWNGRADING SCHEDULE
16. DISTRIBUTION STATEMENT (of this Report) According to attached distribution list. Approved for public release; distribution unrestricted UNLIMITED		
17. DISTRIBUTION STATEMENT (of the abstract entered in Block 20, if different from Report)		
18. SUPPLEMENTARY NOTES Submitted for publication in: <u>Journal of Materials Science</u>		
19. KEY WORDS (Continue on reverse side if necessary and identify by block number) Adhesion, Bond Strength, Compression, Failure, Fracture, Friction, Joints, Rubber, Seizure, Tension, Testing, Torsion.		
20. ABSTRACT (Continue on reverse side if necessary and identify by block number) A simple theoretical analysis, based upon Griffith's fracture criterion, has been developed to predict the loads required to cause adhesive failure when model joints are subjected to different types of loading, viz. tension, compression, and torsion. Two model joints are considered: a rigid cylinder partly embedded in and bonded to an elastic cylinder (termed "rod joint" here), and, an elastic cylinder inserted partway into, and bonded to, a rigid tube (termed "sleeve joint" here). Both types of joint have been constructed, using vulcanized rubber cylinders bonded to aluminum rods and sleeves.		

Measurements have been made of the failure loads under tension, compression and torsional loading. They were found to be in satisfactory agreement with the theoretical predictions except, in some instances, for rod joints subjected to tension or torsional loading when the failure loads were as much as three times the predicted values. This discrepancy is attributed to friction between the partially-detached rubber cylinder and the embedded rod, enhanced to a major degree by the tendency of the rubber cylinder to shrink in radius on stretching or twisting. A theoretical analysis of the effect of friction is presented. It predicts increasingly large pull-out forces or torques, as the depth of embedment increases, until frictional seizure occurs. Experimentally, frictional effects were eliminated by applying an internal gas pressure to the region being detached. All of the failure loads were then found to be in satisfactory agreement with the original theory, ignoring frictional effects. Thus, a simple fracture energy criterion is shown to govern the failure of adhesive joints under complex loading conditions, with or without friction acting at the interface.

Accession For	
NTIS GRA&I	<input checked="" type="checkbox"/>
DTIC TAB	<input type="checkbox"/>
Unannounced	<input type="checkbox"/>
Justification	
By _____	
Distribution/	
Availability Codes	
Dist	Avail and/or Special
A	

1. Introduction

In general, the strength of an adhesively-bonded joint is a function of the mode of loading and the dimensions and elastic properties of the bonded components, as well as of the intrinsic strength of the interface. The objective of failure analysis of adhesive joints is to relate the breaking load to these diverse factors. One approach uses a simple energy criterion for fracture, in terms of a characteristic energy for breaking apart the interface. Originally proposed by Griffith [1] for the brittle fracture of solids, an energy criterion for fracture has been successfully applied to the separation of two adhering solids by a number of previous authors (for example [2-13]).

In applying an energy criterion to adhesive failure, it is first necessary to identify an initial point of separation, usually a flaw or point of high stress concentration at the interface between the two adhering solids. Then, failure is assumed to take place by growth of this initial debond until the joint is completely broken. An energy balance is formulated for a small growth of the debond--changes in the strain energy of the joint and the potential energy of the loading device are equated to the characteristic energy needed for debonding. This energy balance provides the required relation between the breaking load, the properties of the two adhering solids and the dimensions of the joint. It has been applied to the debonding of laminates by Kendall [10-12] and to the pull-out of embedded inextensible cords by Gent et al [13].

Relations obtained in this way for the failure load contain no adjustable parameters. Successful prediction of observed failure loads

is therefore strong evidence for the validity of the proposed failure criterion and of the simplifying assumptions made in the analysis, viz., linearly elastic behavior of the adherends and substantially homogeneous deformation of parts of each adherend. Moreover, the predicted failure loads may be used as the basis for rational design of bonded components, once the basic assumptions of the theory have been shown to hold. Furthermore, simple test methods can be developed for determining the characteristic strength of bonded interfaces from the measured failure loads of suitable model joints. The analysis of the pull-out force of cords embedded in rubber blocks [13] has been employed in this way to measure the adhesion of tire cords to rubber [14].

Strong additional support for the basic concept of an energy criterion governing the failure of adhesive joints would be provided by successful analysis of more complex loading conditions. In the present work the analysis of the pull-out force for an embedded rigid cylindrical rod by Gent et al [13] is extended to include compressive and torsional failure loads also, and applied to a reverse geometry, in which a cylindrical rubber rod is partly embedded in, and bonded to, a rigid cylindrical tube or sleeve. The first configuration, shown in Figure 1a, is referred to here as the "rod joint", and the second, shown in Figure 1b, as the "sleeve joint". Experiments on model joints, using a rubber vulcanizate bonded to aluminum rods and sleeves, are then described and the results compared to the predictions of the theoretical analysis. The theory is then extended to include a frictional interaction between the two surfaces, when they are pressed into close contact after debonding.

2. Theoretical considerations

2.1 Rod joint

The following analysis is a generalization of that given by Gent et al [13] to include compressive and torsional failure modes.

A rigid rod, radius a , is partly embedded in and bonded to a rubber cylinder of radius r . Debonding is effected by one of the following means:-

- a) application of a tensile force, F (Figure 2a);
- b) application of a torque, M (Figure 2a);
- c) application of a compressive force, F (Figure 2b).

Note that for the compressive experiments a hole was provided in the rubber cylinder to accommodate the displacement of the rod, as shown schematically in Figure 2b.

Debonding is expected to initiate quite easily at the embedded end of the rod because of the high stress concentration there. Consider the situation after a small debond of length x has developed. The rubber cylinder may then be regarded as made up of three regions, viz:-

Region A - This part is still bonded to the rod. It is assumed that the rubber in this region is unstrained.

Region B - This part, in the form of a tube of length x , is no longer bonded to the rod. It is assumed that the rubber in this region is in a state of simple extension, compression, or torsion depending on the type of loading.

Region C - The end region is assumed to be substantially in simple extension, ^{compression} or torsion; however, its exact state of deformation does not enter into consideration as long as it remains constant under a constant (failure) load.

Propagation of the debond by a small amount Δx results in the growth of Region B by an amount Δx at the expense of Region A. Thus, the volume of rubber subjected to strain increases by an amount $\pi(r^2 - a^2)\Delta x$ and the total strain energy of the joint increases correspondingly. However, the potential energy of the loading device decreases. The difference between the energy supplied by the loading device and the gain in strain energy is the energy available for fracture. For debond propagation, this energy must equal or exceed the energy requirement for fracture, i.e., $2\pi a \Delta x G_a$, where G_a is the characteristic energy required to fracture unit area of the adhesive interface.

The energy balance equation can be written explicitly provided the stress/strain properties of the rubber are known. For simplicity, it is first assumed that the rubber is linearly elastic with Young's modulus E and a shear modulus equal to $E/3$.

For tension and compression, the energy supplied by the load F is $F e \Delta x$ where e is the strain in Region B, given by $e = F / \pi (r^2 - a^2) E$. The increase in strain energy is $\frac{1}{2} F e \Delta x$ or half the work done by the load. Hence for debond propagation,

$$\frac{1}{2} F e \Delta x > 2\pi a \Delta x G_a$$

Thus the relation between G_a and the failure force F_f in tension or compression is (13)

$$G_a = \frac{F_f^2}{4\pi^2 a (r^2 - a^2) E} \quad (\text{Eq. 1})$$

For torsion, the energy supplied by the applied torque M is $M \Delta \theta$ where $\Delta \theta$ is the increase in the angle of twist resulting from a debond propagation of Δx . The increase in strain

energy is $\frac{1}{2} M \Delta\theta$, and hence for debond propagation,

$$\frac{1}{2} M \Delta\theta > 2\pi a \Delta x G_a.$$

But from elasticity theory, $\Delta\theta$ is given by

$$\Delta\theta = \frac{6 M \Delta x}{\pi (r^4 - a^4) E}$$

Thus, the predicted relation between G_a and the failure torque M_f is

$$G_a = \frac{3 M_f^2}{2\pi^2 a (r^4 - a^4) E} \quad (\text{Eq. 2})$$

2.2 Sleeve joint

A rubber cylinder, radius a , is partly embedded within, and bonded to, a rigid sleeve (Figure 3). Debonding is again effected by either

- a) application of a tensile force, F , or,
- b) application of a torque, M .

In these cases, debonding is expected to initiate at the rim of the sleeve where the rubber cylinder enters it. After a small debond of length x has developed, the rubber cylinder may again be regarded as made up of three regions, viz:-

Region A - Where the rubber is still bonded to the sleeve and is assumed to be unstrained.

Region B - Of length x , where the rubber has become debonded and is assumed to be in a state of simple extension or torsion.

Region C - Assumed to remain in a state of simple extension or torsion under the applied load or torque.

Propagation of the debond by a small amount Δx results in the growth of Region B by Δx at the expense of Region A.

Writing the energy balance equation as before yields the result in tension

$$G_a = \frac{F_f^2}{4\pi^2 a^3 E} \quad (\text{Eq. 3})$$

and in torsion

$$G_a = \frac{3M_f^2}{2\pi^2 a^3 E} \quad (\text{Eq. 4})$$

2.3 Non-linear elasticity

The assumption of linear elasticity of rubber made in the above analysis is strictly valid only at very small strains (eg. up to about 10% in tension or compression). If adhesive failure occurs when the rubber is subjected to higher strains, then the relations obtained will be in error by an amount dependent upon the degree of departure from linearity.

Some increase in accuracy can be obtained by assuming that the rubber obeys the statistical theory of rubber elasticity. It is known that the statistical theory gives a fairly good description of the stress/strain behavior of well-vulcanized rubber up to moderate strains, about 50% in tension or compression [15]. Moreover, a rubber obeying the statistical theory behaves substantially linearly in torsion [15]. Thus, equations 2 and 4 are expected to apply for relatively large torsional strains.

Equations corresponding to equations 1 and 3 can be readily derived for a rubber obeying the statistical theory. It has been shown above that the energy available for debond propagation is the difference between the work done by the applied load and the gain in stored energy. This available energy is represented in Figure 4 by the shaded areas.

For a non-linearly elastic rubber, Figure 4b, the available energy is underestimated in tension but overestimated in compression if linear elasticity is assumed.

The energy available for debond propagation Δx is $\frac{A\Delta x}{\pi a^2} \int e \, d\sigma$ where A is the cross-sectional area of the rubber (equal to $\pi(r^2 - a^2)$ for the rod joint and πa^2 for the sleeve joint) and σ is the applied stress, equal to F/A (positive for tension and negative for compression).

For a rubber obeying the statistical theory, the stress/strain relation in tension/compression can be expressed as the power series

$$e = \frac{\sigma}{E} + \left(\frac{\sigma}{E}\right)^2 + \frac{2}{3}\left(\frac{\sigma}{E}\right)^3 + \dots$$

Hence the criterion for debond propagation becomes

$$A\Delta x \frac{\sigma^2}{2E} \left\{ 1 + \frac{2}{3}\left(\frac{\sigma}{E}\right) + \frac{1}{3}\left(\frac{\sigma}{E}\right)^2 + \dots \right\} > 2\pi a \Delta x G_a$$

For the rod joint, the relation between G_a and the failure load F_f is then

$$G_a = \frac{F_f^2}{4\pi^2 a (r^2 - a^2) E} \left\{ 1 + \frac{2}{3}\left(\frac{\sigma}{E}\right) + \frac{1}{3}\left(\frac{\sigma}{E}\right)^2 + \dots \right\} \quad (\text{Eq. 1a})$$

and for the sleeve joint

$$G_a = \frac{F_f^2}{4\pi^2 a^3 E} \left\{ 1 + \frac{2}{3}\left(\frac{\sigma}{E}\right) + \frac{1}{3}\left(\frac{\sigma}{E}\right)^2 + \dots \right\} \quad (\text{Eq. 3a})$$

2.4 Testing the theory

The above analysis has yielded theoretical relations for the fracture loads in five possible experimental configurations. The equations derived have no adjustable parameters. The characteristic failure energy G_a , may thus be compared within this group of five experiments and it may also be determined independently in a peeling

experiment. Agreement of the results from such varied experiments may be regarded as a rather stringent test of the applicability of the Griffith fracture energy criterion to the failure of adhesive joints. Furthermore, employing the same joint for experiments under different modes of loading avoids some of the experimental uncertainties associated with different sample preparations.

3. Experimental details

3.1 Materials

Rubber cylinders were prepared by a hot molding process using the following mix formulation in parts by weight: natural rubber, 100; zinc oxide, 5; stearic acid, 2; sulfur, 2.5; N-cyclohexyl - 2 - benzothiazylsulfenamide, 0.6. Vulcanization was effected by heating for 45 minutes at 140°C. From the initial slope of the stress-strain relation of tall cylindrical specimens compressed between lubricated platens, Young's modulus E was found to be 1.75 MPa.

A proprietary adhesive, Chemlok 205 (supplied by Hughson Chemicals, Lord Corporation) was used for bonding the rubber to aluminum rods and sleeves during vulcanization. Although this adhesive is not normally recommended for use alone with natural rubber, it gives a bond of moderate strength, yet weak enough so that apparent interfacial failure is obtained consistently. Other adhesives, such as Chemlok 220, are normally used with natural rubber but they generally give a much stronger bond so that the rubber tears rather than detaches from the substrate.

3.2 Test pieces

Rod and sleeve joints were prepared by vulcanizing the rubber in a transfer mould with appropriate aluminum inserts serving as the adherends. The aluminum adherends were prepared by machining them to size, polishing them with silicon carbide paper and then cleaning them with acetone before the Chemlok 205 adhesive was painted onto the curved surfaces and allowed to dry. The aluminum parts were then

inserted into the mold before the rubber mix was injected and vulcanized in situ. For the rod joint, the rubber cylinder had a radius r of 12.4 mm. and a length of 35 mm. The aluminum rod had an embedded length of 20 mm. Rods of various radii, in the range 0.85 to 7.5 mm., were employed but most of the experiments were carried out with rods of 5 mm. radius.

For rod joints intended for testing in compression, an end piece and rod without any adhesive was used at one end of the specimen to form the central hole and flat end. For other test pieces, a flat aluminum end-piece painted with Chemlok 220 was used at one end. This facilitated gripping of the end of the specimen during testing and use of the stronger Chemlok 220 adhesive insured that premature failure did not occur at this end.

For the sleeve joint, the aluminum sleeve had a length of 35 or 15 mm. and an internal radius ranging from 6.35 to 11.35 mm. The external radius of the rubber cylinder was the same as the internal radius of the sleeve.

To determine the adhesive fracture energy G_a independently, a peel test piece was used, consisting of a strip of rubber, 25 mm. wide, 75 mm. long, and 1.5 mm. thick, bonded to an aluminum plate with the same Chemlok 205 adhesive.

3.3 Test procedures

All experiments were performed at room temperature, using an Instron universal testing machine. For torsion tests, a simple pulley

system was used to convert the vertical movement of the machine cross-head to a rotation of the test piece.

Peeling experiments were performed at a stripping angle of 90° and at speeds of 0.5, 5 and 50 mm/min. All other experiments were performed at a crosshead speed of 5 mm/min. With the pulley system used, this corresponds to about 25×10^{-3} radians/min. for the torsion experiment.

4. Results and discussion

4.1 Determination of G_a

Table 1 gives the results obtained from peeling experiments. The characteristic energy G_a for adhesive failure was calculated from the relation

$$G_a = F_p/w$$

where F_p is the steady peel force and w is the width of the adhering strip. It is seen from the results that this particular experimental system has an unexpected advantage -- the bond strength is only moderately sensitive to the rate of detachment. The mean value for G_a , about 140 J/m² is taken here as representative of the interfacial bond strength at moderate rates of detachment and at ambient temperatures.

4.2 Sleeve joint

The theory developed earlier predicts that the failure force or failure torque will be independent of the length of the joint. This means that a constant failure force or torque is to be expected. This is observed in practice with the sleeve joint. Once failure has been initiated, it continues at constant force or torque.

The results obtained for the failure forces and torques with the sleeve joint under tension or torsion are summarized in Table 2. Values of G_a have been calculated from them using equations (3a) and (4).

It is seen from Table 2 that the values of G_a obtained in this way ranging from 104-180 J/m², are in fairly good agreement with each other and with the value obtained from the peel experiments (about 140 J/m²).

Considering the very different deformations applied to the joints and the fact that the equations used to calculate G_a have no adjustable parameters and rather strong and different dependences on the radius a of the specimen, this agreement is regarded as quite satisfactory. However, there is some indication that larger values of G_a are obtained with specimens of larger radius. This may be due to the relatively small length of the bonded part of the specimens in these cases. One assumption of the theoretical analysis, that the bonded part of the specimen is effectively unstrained, will cease to hold when the radius of the cylinder becomes comparable in size to the length of the bonded part.

4.3 Rod joint

The failure of a rod joint was found to take place quite differently in tension and in torsion, than in compression. Experiments in compression with an embedded aluminum rod of 5 mm. radius gave values for the failure force of 94 ± 11 N and hence a value for the effective fracture energy G_a of 184 ± 39 J/m², in reasonably good agreement with values obtained previously. However, in both tension and torsion, no well-defined failure load was observed. Instead, the tensile force or torque increased continuously during the experiment until catastrophic failure took place. Examination of the recorded plots of load vs time often showed a discontinuity at loads less than the final fracture load, when bond failure may have been initiated, but this point was not well-defined and much larger loads were require to cause fracture of the joint. The final breaking force or torque has been taken here as the failure load.

Values of the failure loads in tension and torsion are given in Table 3 for a rod joint having an embedded rod of 5 mm. radius. Values of the apparent fracture energy G_a calculated from the observed failure loads are also given in Table 3. They are seen to be much greater than before. Measurements with embedded rods of different radii are reported in Table 4. They reveal that the apparent fracture energy increases as the radius of the embedded rod increases. Only for rods of relatively small radius are the calculated fracture energies comparable to those obtained previously; otherwise, they are considerably larger. Clearly, a significant factor has been omitted from the theoretical analysis for the cases of a rod joint subjected to tension or torsional loading, and this factor becomes increasingly important as the radius of the embedded rod is increased. It is attributed to frictional effects, for the following reasons.

Referring to the sketch in Figure 2a, it has been assumed that a region B of debond develops during tension or torsional failure of a rod joint. This region is essentially a rubber tube, placed in tension or torsion by the applied forces after debonding. Now, on stretching a rubber tube, the radius tends to undergo Poissonian contraction, and there is a similar tendency for the radius to shrink when a tube is subjected to torsion [16,17]. Thus, for a rod joint under tension or torsional loading the debonded tube will tend to grip the embedded rod tightly and increase any frictional forces acting at the interface. On the other hand, for a rod joint under compressive loads, Figure 2b, the rubber tube formed by debonding will tend to spread outwards away from the embedded rod, so that frictional effects should be absent in this

case. Similarly, for a sleeve joint subjected to tension or torsional loads, contraction of the rubber cylinder after debonding will cause it to move away from the surrounding rigid sleeve and frictional effects will again be absent.

Thus, the two test configurations which give rise to anomalously high failure loads and hence high effective fracture energies, are also those for which the rubber section is pressed into close contact with the rigid inclusion after debonding. An approximate theoretical treatment of the corresponding frictional contribution to the work of detachment is given in the next section of this paper, and some experiments designed to minimize frictional effects during tension and torsional fracture of rod joints are described in the following section.

5. Frictional contribution to the fracture energy for a rod joint subjected to tension or torsion

5.1 Theoretical considerations

A rather approximate estimate of the contribution to the failure loads from friction can be made, as follows. It is assumed that the frictional stress τ is uniform over the debonded region (B in Figure 2a) and given by

$$\tau = \mu P$$

where μ is the coefficient of friction and P is the normal pressure acting on the embedded rod. The frictional force resisting pull-out, acting over the region B, is therefore given by $2\pi ax\mu P$ and the additional work required to cause an incremental debond of length Δx is $2\pi ax\mu P \Delta x$.

Thus, the energy balance equation now becomes:

$$F^2/2\pi (r^2-a^2)E > 2\pi aG_a + 2\pi ax\mu P e.$$

The tensile strain e of the debonded rubber is given by $F/\pi (r^2-a^2)E$ and the pressure P is given, for small strains, by the relation [16,17]:

$$P = (r^2-a^2) Ee/3r^2.$$

On substituting for P and e in terms of the applied load F , the pull-out force in the presence of friction is obtained in the form

$$F^2 = 4\pi^2 a (r^2-a^2) E G_a / [1 - (4a\mu x/3r^2)].$$

It is clear that the pull-out force is increased by friction and that it becomes larger as debonding continues, i.e., as \underline{x} increases, so that the force required to propagate the debond rises continuously, rather than remaining constant. This is in accord with observation. Indeed, the pull-out force is predicted to become infinitely large when the debonded length \underline{x} reaches a critical value \underline{x}_c , given by

$$x_c = 3r^2/4a\mu .$$

Thus, for thin-walled rubber tubes, a rod embedded to a depth much greater than its radius will be gripped by friction to such a degree that, even in the absence of bonding, pull-out will be impossible. The critical embedment depth \underline{x}_c for thick-walled tubes is predicted to be considerably larger, however.

Previous studies of the pull-out force for embedded cords dealt with relatively small-radius cords [13]. In such cases, frictional contributions to the observed failure loads would be expected to be small, unless the cords were embedded to great depths, approaching \underline{x}_c .

Similar considerations apply to the torsional failure of a rod joint in the presence of friction. In this case the additional work required to cause an incremental debond of length $\underline{\Delta x}$ is $\underline{2\pi a^2 \mu P \theta \Delta x}$, where $\theta = 6Mx / \pi(r^4 - a^4)E$.

The energy balance equation then becomes:

$$3M^2/\pi(r^4 - a^4)E > 2\pi a G_a + 2\pi a^2 \mu P \theta .$$

On substituting for θ in terms of M , and for pressure P from the relation [16,17],

$$P = E(r^2 - a^2)\theta^2/6x^2,$$

the failure torque M in the presence of friction is given by the following implicit relation:

$$M^2 = \frac{2}{3}\pi^2 a(r^4 - a^4)E G_a + 24a^2\mu(r^2 - a^2)x M^3/\pi(r^4 - a^4)^2 E.$$

At a critical value of the debond length x , denoted x_c , the failure torque is entirely accounted for by friction, even in the absence of any bonding ($G_a = 0$).

The corresponding torque, denoted M_c , is the maximum that could give rise to further debonding. If the applied torque exceeds this value, then the work expended in frictional sliding would exceed that available so that no motion is possible. The critical torque is given by

$$M_c = \pi a^4 \left(\frac{r^2}{a^2} + 1\right)^2 \left(\frac{r^2}{a^2} - 1\right) E / 24\mu x$$

and the corresponding angle of rotation θ_c by

$$\theta_c = \left(\frac{r^2}{a^2} + 1\right) / 4\mu.$$

The above theoretical considerations reveal that frictional effects will become important, and eventually dominant, for the rod joint when the rod diameter becomes comparable to the wall thickness of the rubber tube surrounding it, and when the depth of embedment is sufficiently large. Under these circumstances frictional seizure is predicted to occur. (The same principle is employed in Chinese finger cuffs: extensible tubes which grip the fingers more firmly the harder one tries to pull them out.) In the following section, experiments are described that were designed to minimize frictional effects in rod joints, and for which the original theoretical treatment, neglecting friction, should hold.

5.2 Use of internal gas pressure to minimize friction in rod joints

A small hole was drilled along the axis of the embedded aluminum rod to permit the application of nitrogen gas under pressure to the interface during a debonding experiment. This pressure was then maintained constant during the application of tension or torsional loads. Failure loads were determined in this way at various values of applied internal pressure for specimens with an embedded rod of 5 mm. radius. The results are shown graphically in Figure 5 and 6.

As would be expected when an internal gas pressure is applied, tending to hold the debonded rubber away from the embedded rod, the measured failure loads were much smaller than before. They fell rapidly as the internal pressure was increased from zero up to a pressure of about 100 kPa. Above this pressure, further increases in pressure had a smaller effect. Eventually, at a pressure of about 400 kPa the bond failed under the action of the gas pressure alone, without any additional load being applied.

It is assumed that the initial rapid fall in failure force or failure torque with applied pressure is due to a concurrent reduction in friction, and at the critical pressure, about 100 kPa it is assumed that frictional effects have been virtually overcome. Slow further reductions in failure loads with further increases in gas pressure are attributed to a direct contribution to the strain energy employed in debonding from the applied pressure itself.

By extrapolating the relations observed at pressures greater than about 100 kPa, when frictional effects are assumed to be absent, back

to zero pressure, as shown by the broken lines in Figures 5 and 6, values for the failure loads in the absence of friction were estimated. The values obtained in this way were a pull-out force of 100N and a failure torque of 0.68 Nm, corresponding to values of the fracture energy G_a of 250 J/m² and 350 J/m², respectively. These values are in approximate agreement with those obtained previously from compression experiments on rod joints, and from tension and torsion experiments on sleeve joints, indicating that the applied pressure had, indeed, eliminated the frictional contribution to the work of fracture.

6. Conclusions

The applicability of the Griffith fracture criterion to the failure of adhesive bonds has been subjected to a severe test. Two model joints have been examined under tension, compression and torsional loading and the measured failure loads compared to the theoretically - predicted values. Satisfactory agreement was obtained in all cases, except where frictional effects are significant; i.e., for a rod joint subjected to tension or torsion. When the theory is amended to take into account friction between the debonded surfaces, enhanced by the pressure generated indirectly by the applied load, then the observed increase in failure loads for rod joints is fully accounted for. Indeed, frictional seizure is predicted to occur for deeply embedded rods. Even in the absence of bonding, the load to pull out or twist free such rods is predicted to be infinitely large, due to the self-reinforcing nature of the frictional resistance.

References

1. A. A. Griffith, Philos. Trans. Roy. Soc. (Lond.) 221, 163-198 (1920).
2. R. S. Rivlin, Paint Technol. 9, 215-218 (1944).
3. B. V. Deryagin and N. A. Krotova, Dokl. Akad. Nauk. SSSR 61, 849-851 (1948).
4. E. J. Ripling, S. Mostovoy and R. L. Patrick, Mater. Res. Stand. 4, 129-134 (1963).
5. B. M. Malyshev and R. L. Salganik, Int. J. Fracture Mech. 1, 114-128 (1965).
6. M. L. Williams, Proc. 5th U. S. Natl. Congress on Applied Mechanics, Minneapolis, June, 1966, American Society of Mechanical Engineers, New York, 1966, pp. 451-464.
7. A. N. Gent and A. J. Kinloch, J. Polymer Sci. Part A-2 9, 659-668 (1971).
8. P. B. Lindley, J. Inst. Rubber Industry 5, 243-248 (1971).
9. W. D. Bascom, R. L. Cottingham, R. L. Jones and P. Peyser, J. Appl. Polymer Sci. 19, 2545-2562 (1975).
10. K. Kendall, J. Phys. D: Appl. Phys. 4, 1186-1195 (1971).
11. K. Kendall, J. Phys. D: Appl. Phys. 8, 512-522 (1975).
12. K. Kendall, J. Materials Sci. 11, 638-644 (1976).
13. A. N. Gent, G. S. Fielding - Russell, D. I. Livingston and D. W. Nicholson, J. Materials Sci. 16, 949-956 (1981)
14. G. S. Fielding - Russell, D. W. Nicholson and D. I. Livingston in "Tire Reinforcement and Tire Performance", ASTM STP 694, ed. by R. A. Fleming and D. I. Livingston, American Society for Testing

- and Materials, Philadelphia, 1979, pp. 153-162.
15. L. R. G. Treloar, *The Physics of Rubber Elasticity*, 3rd. ed., Clarendon Press, Oxford, 1975.
 16. R. S. Rivlin, *Philos. Trans. Roy. Soc. (Lond.)* A242, 173-195 (1949)
 17. A. N. Gent and R. S. Rivlin, *Proc. Phys. Soc. (Lond.)* 65B, 487-501 (1952).

TABLE 1 RESULTS FROM PEELING EXPERIMENTS

<u>SPEED (mm/min)</u>	<u>G_a (J/m²)</u>
0.5	119 ± 10
5	143 ± 12
50	173 ± 20

TABLE 2 RESULTS FOR SLEEVE JOINTS

<u>radius</u>	<u>length</u>	<u>Tension</u>		<u>Torsion</u>	
(mm)	(mm)	<u>F_f (N)</u>	<u>G_a (J/m²)</u>	<u>M_f (N.m)</u>	<u>G_a (J/m²)</u>
6.35	15	40 ± 2	104 ± 11	0.112 ± 0.007	106 ± 14
6.35	35	42 ± 2	112 ± 12	0.112 ± 0.005	106 ± 9
9.55	35	77 ± 2	109 ± 5	0.343 ± 0.005	129 ± 4
11.35	35	113 ± 11	141 ± 28	0.626 ± 0.013	180 ± 8

TABLE 3 RESULTS FOR ROD JOINTS (ROD RADIUS: 5 mm.)

<u>Mode of deformation</u>	<u>Failure load</u>	<u>G_a (J/m²)</u>
Tension	250 ± 49 N	1880 ± 810
Compression	94 ± 11 N	184 ± 39
Torsion	1.18 ± 0.20 N.m	1060 ± 380

TABLE 4 RESULTS FOR ROD JOINTS (RODS OF DIFFERENT RADII)

<u>Rod radius</u> <u>a (mm)</u>	<u>Tension</u>		<u>Torsion</u>	
	<u>F_f (N)</u>	<u>G_a (J/m²)</u>	<u>M_f (N.m)</u>	<u>G_a (J/m²)</u>
0.85	60 ± 5	430 ± 80	-	-
1.2	79 ± 12	540 ± 170	-	-
2.5	179 ± 13	1470 ± 230	0.38 ± 0.08	220 ± 84
5.0	250 ± 49	1880 ± 810	1.18 ± 0.20	1060 ± 380
7.5	346 ± 31	3770 ± 890	> 2	> 2000

FIGURE LEGENDS

FIGURE 1. Sketch of model joints

(a) rod joint

(b) sleeve joint

Rigid parts shown shaded, elastic parts not shaded.

FIGURE 2. Rod joint

(a) tension or torsion

(b) compression (note hole to accommodate displacement of the rod)

Rigid parts shown shaded, elastic parts not shaded.

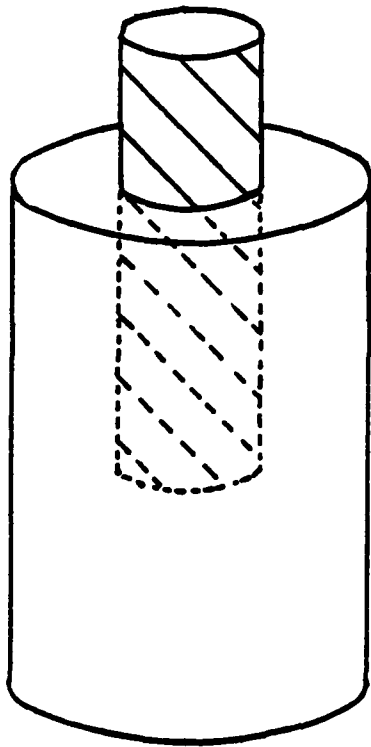
FIGURE 3. Sleeve joint

Rigid parts shown shaded, elastic parts not shaded.

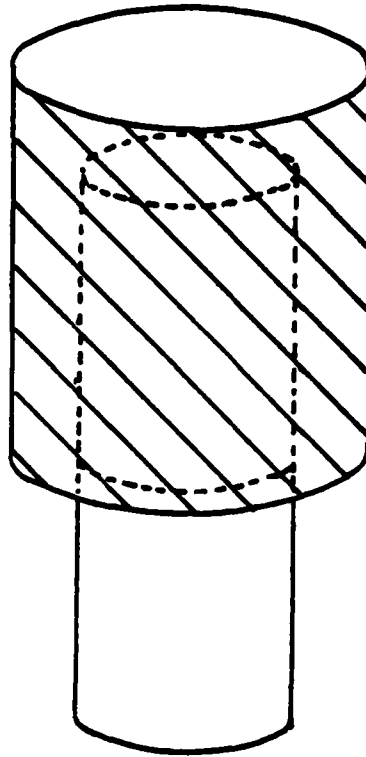
FIGURE 4. Schematic diagram showing energy available for debond propagation. Shaded area represents available energy.

FIGURE 5. Dependence of pull-out force on internal pressure

FIGURE 6. Dependence of failure torque on internal pressure.



(a)



(b)

Figure 1

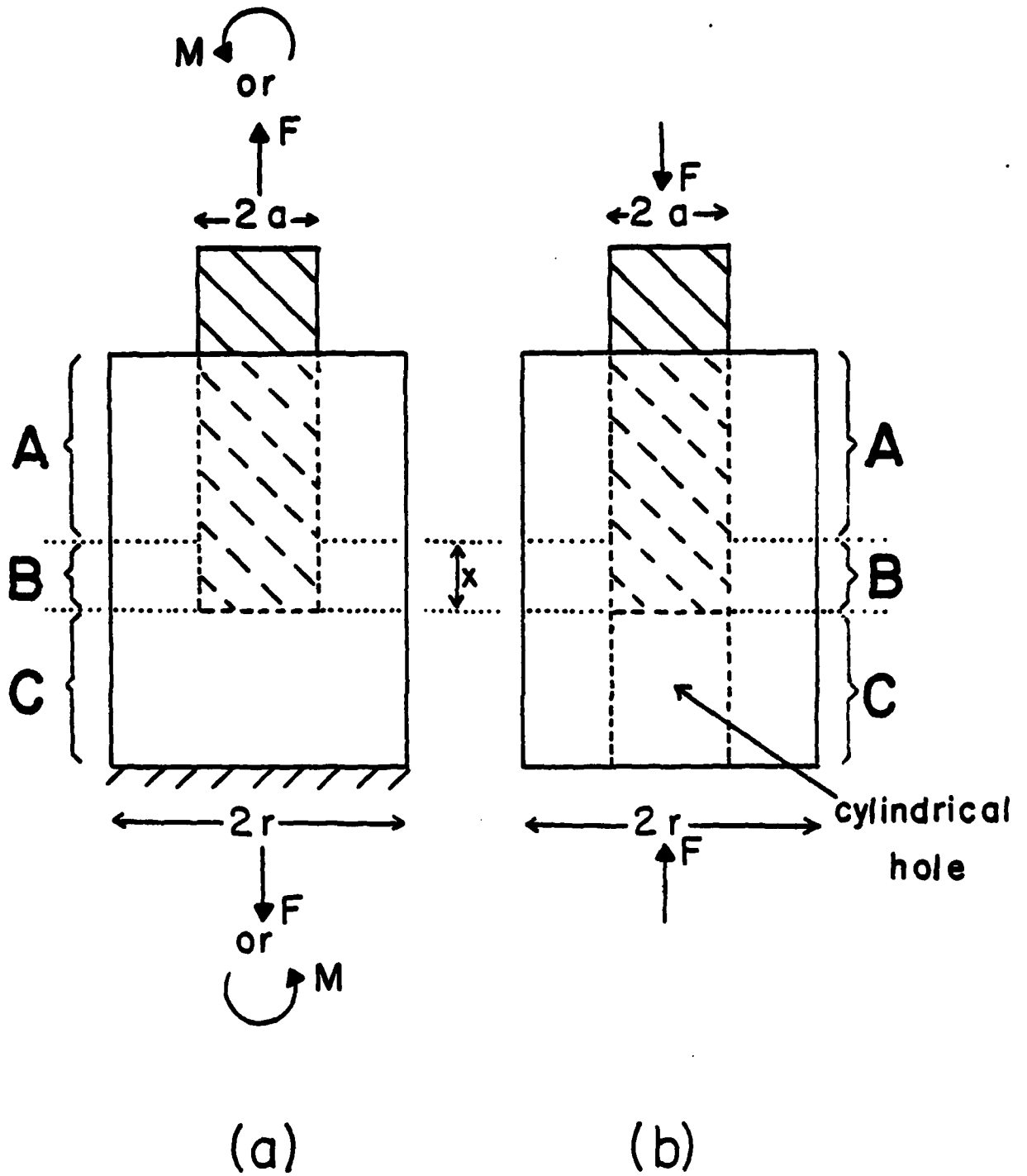


Figure 2

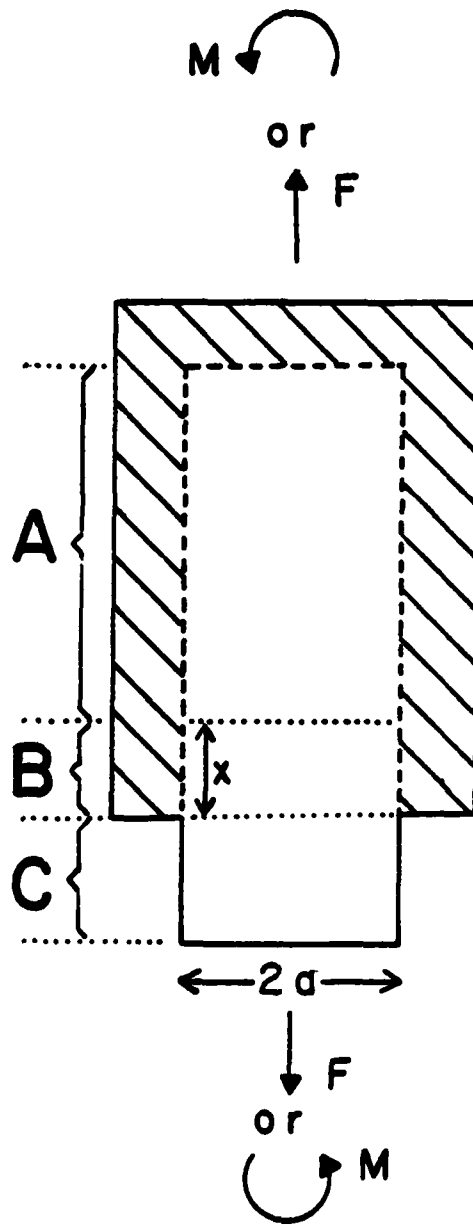


Figure 3

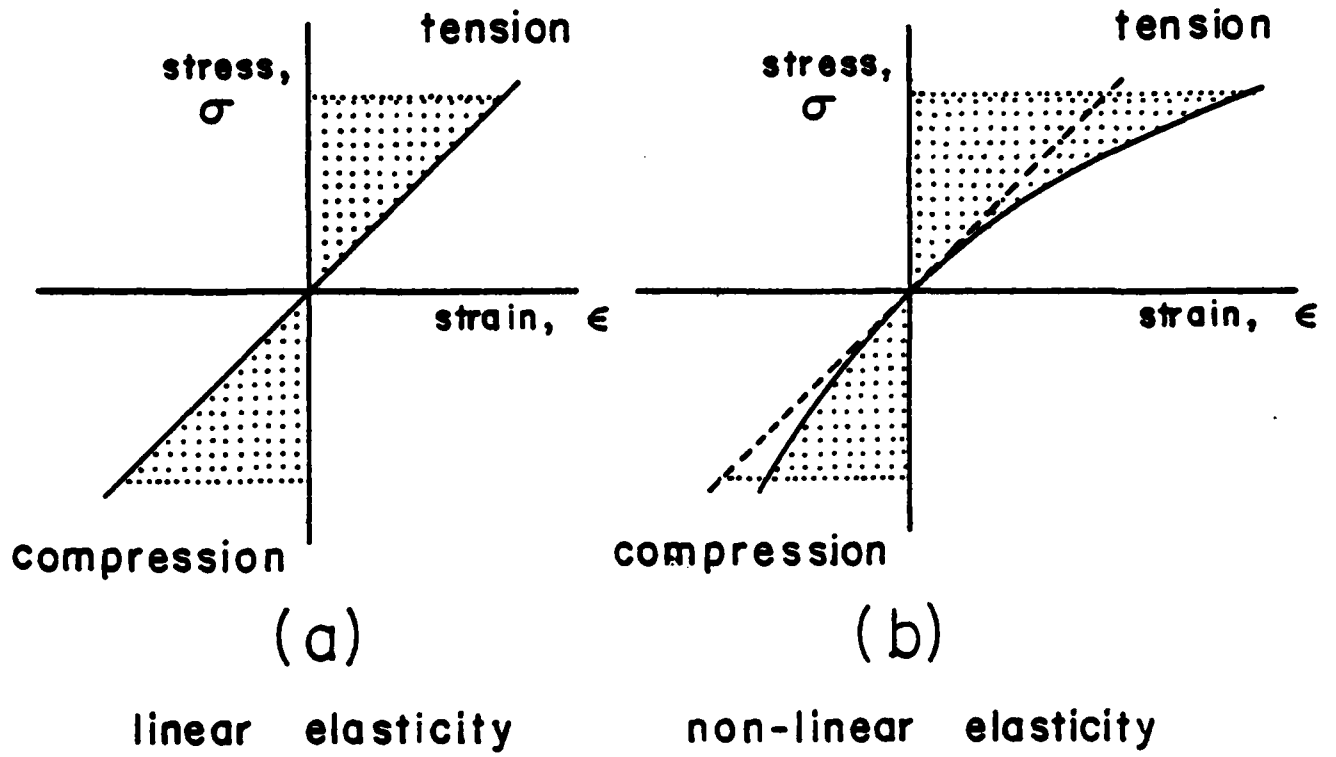


Figure 4

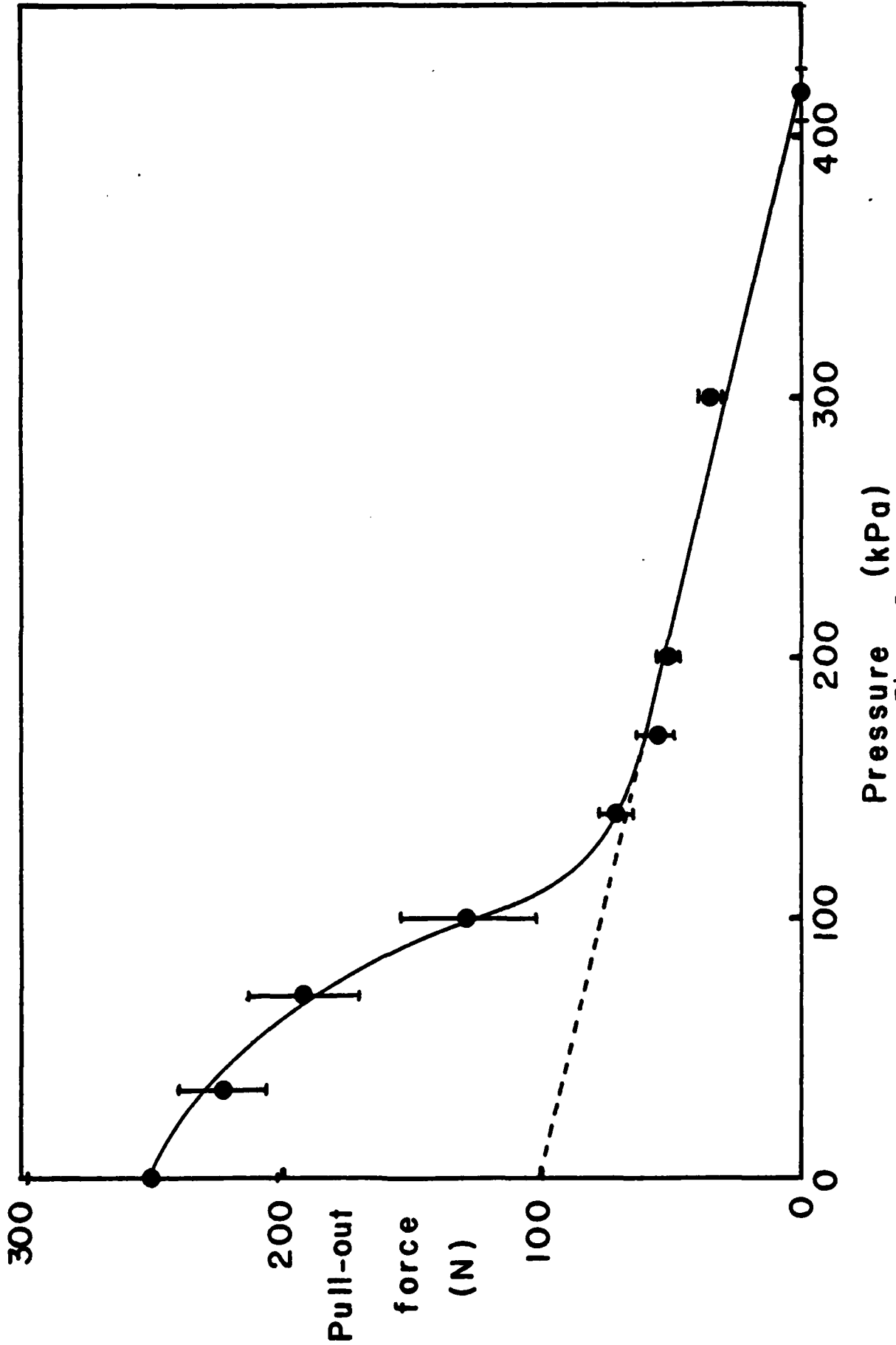
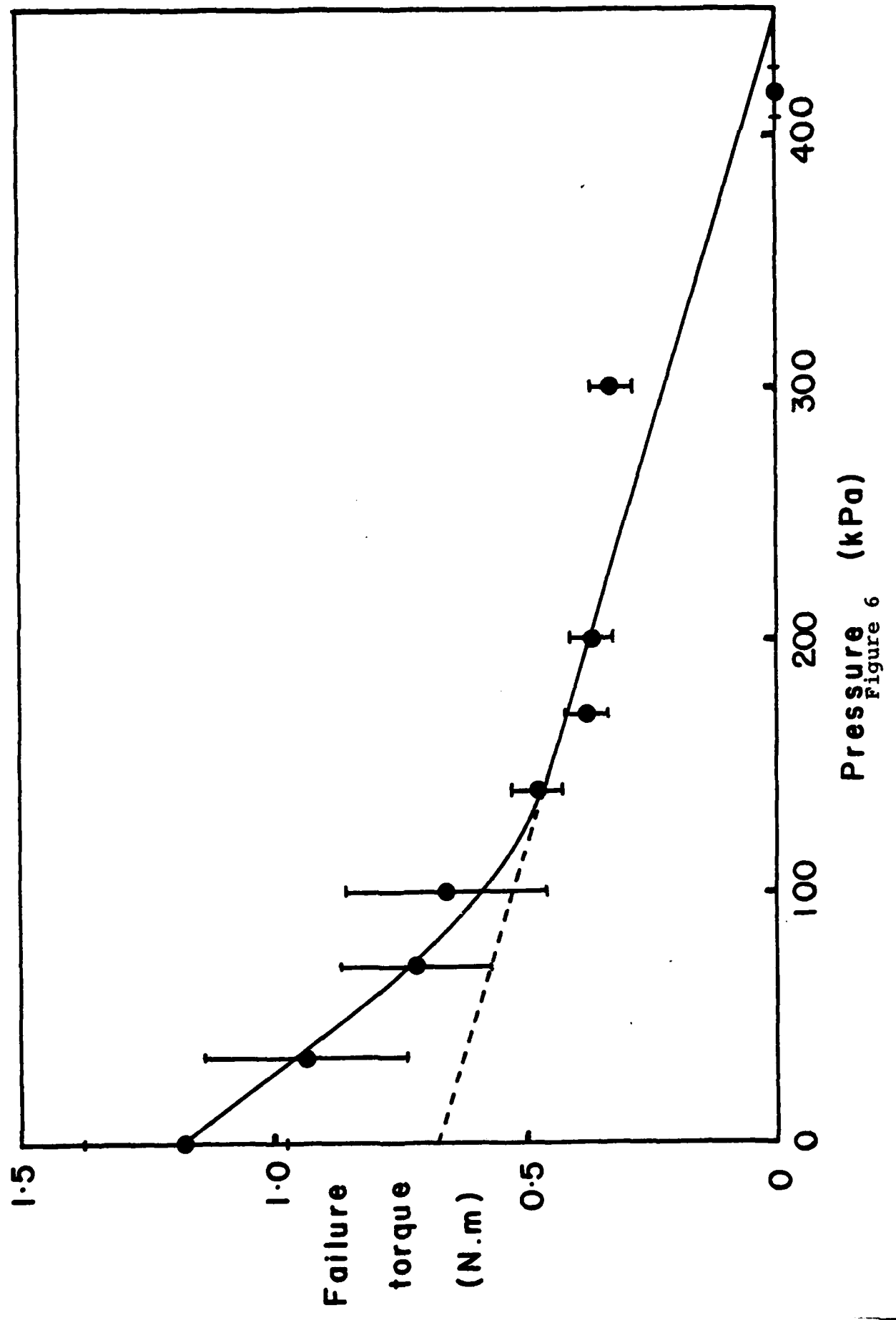


Figure 5



Pressure (kPa)
Figure 6

Failure torque (N.m)

DISTRIBUTION LIST

	<u>No. Copies</u>		<u>No. Copies</u>
Dr. L.V. Schmidt Assistant Secretary of the Navy (R.E. and S) Room 5E 731 Pentagon Washington, D.C. 20350	1	Dr. F. Roberto Code AFRPL MKPA Edwards AFB, CA 93523	1
Dr. A.L. Slafkosky Scientific Advisor Commandant of the Marine Corps Code RD-1 Washington, D.C. 20380	1	Dr. L.H. Caveny Air Force Office of Scientific Research Directorate of Aerospace Sciences Bolling Air Force Base Washington, D.C. 20332	1
Dr. Richard S. Miller Office of Naval Research Code 413 Arlington, VA 22217	10	Mr. Donald L. Ball Air Force Office of Scientific Research Directorate of Chemical Sciences Bolling Air Force Base Washington, D.C. 20332	1
Mr. David Siegel Office of Naval Research Code 260 Arlington, VA 22217	1	Dr. John S. Wilkes, Jr. FJSRL/NC USAF Academy, CO 80840	1
Dr. R.J. Marcus Office of Naval Research Western Office 1030 East Green Street Pasadena, CA 91106	1	Dr. R.L. Lou Aerojet Strategic Propulsion Co. P.O. Box 15699C Sacramento, CA 95813	1
Dr. Larry Peebles Office of Naval Research East Central Regional Office 666 Summer Street, Bldg. 114-D Boston, MA 02210	1	Dr. V.J. Keenan Anal-Syn Lab Inc. P.O. Box 547 Paoli, PA 19301	1
Dr. Phillip A. Miller Office of Naval Research San Francisco Area Office One Hallidie Plaza, Suite 601 San Francisco, CA 94102	1	Dr. Philip Howe Army Ballistic Research Labs ARRADCOM Code DRDAR-BLT Aberdeen Proving Ground, MD 21005	1
Mr. Otto K. Heiney AFATL - DLDL Elgin AFB, FL 32542	1	Mr. L.A. Watermeier Army Ballistic Research Labs ARRADCOM Code DRDAR-BLI Aberdeen Proving Ground, MD 21005	1
Mr. R. Geisler ATTN: MKP/MS24 AFRPL Edwards AFB, CA 93523	1	Dr. W.W. Wharton Attn: DRSIII-RKL Commander U.S. Army Missile Command Redstone Arsenal, AL 35898	1

DISTRIBUTION LIST

	<u>No. Copies</u>		<u>No. Copies</u>
Dr. R.G. Rhoades Commander Army Missile Command DRSMI-R Redstone Arsenal, AL 35898	1	Dr. E.H. Debutts Hercules Inc. Baccus Works P.O. Box 98 Magna, UT 84044	1
Dr. W.D. Stephens Atlantic Research Corp. Pine Ridge Plant 7511 Wellington Rd. Gainesville, VA 22065	1	Dr. James H. Thacher Hercules Inc. Magna Baccus Works P.O. Box 98 Magna, UT 84044	1
Dr. A.W. Barrows Ballistic Research Laboratory USA ARRADCOM DRDAR-BLP Aberdeen Proving Ground, MD 21005	1	Mr. Theodore M. Gilliland Johns Hopkins University APL Chemical Propulsion Info. Agency Johns Hopkins Road Laurel, MD 20810	1
Dr. C.M. Frey Chemical Systems Division P.O. Box 358 Sunnyvale, CA 94086	1	Dr. R. McGuire Lawrence Livermore Laboratory University of California Code L-324 Livermore, CA 94550	1
Professor F. Rodriguez Cornell University School of Chemical Engineering Olin Hall, Ithaca, N.Y. 14853	1	Dr. Jack Linsk Lockheed Missiles & Space Co. P.O. Box 504 Code Org. 83-10, Bldg. 154 Sunnyvale, CA 94088	1
Defense Technical Information Center DTIC-DDA-2 Cameron Station Alexandria, VA 22314	12	Dr. B.G. Craig Los Alamos National Lab P.O. Box 1663 NSP/DDO, MS-245 Los Alamos, NM 87545	1
Dr. Rocco C. Musso Hercules Aerospace Division Hercules Incorporated Alleghany Ballistic Lab P.O. Box 210 Washington, D.C. 21502	1	Dr. R.L. Rabie WX-2, MS-952 Los Alamos National Lab. P.O. Box 1663 Los Alamos NM 37545	1
Dr. Ronald L. Simmons Hercules Inc. Eglin AFATL/DL0L Eglin AFB, FL 32542	1	Dr. R. Rogers, WX-2 Los Alamos Scientific Lab. P.O. Box 1663 Los Alamos, NM 87545	1

DYN

6/81

DISTRIBUTION LIST

	<u>No. Copies</u>		<u>No. Copies</u>
Mr. R. Brown Naval Air Systems Command Code 330 Washington, D.C. 20361	1	Dr. J. Schnur Naval Research Lab. Code 6510 Washington, D.C. 20375	1
Dr. H. Rosenwasser Naval Air Systems Command AIR-310C Washington, D.C. 20360	1	Mr. R. Beauregard Naval Sea Systems Command SEA 64E Washington, D.C. 20362	1
Mr. B. Sobers Naval Air Systems Command Code 03P25 Washington, D.C. 20360	1	Mr. G. Edwards Naval Sea Systems Command Code 62R3 Washington, D.C. 20362	1
Dr. L.R. Rothstein Assistant Director Naval Explosives Dev. Engineering Dept. Naval Weapons Station Yorktown, VA 23691	1	Mr. John Boyle Materials Branch Naval Ship Engineering Center Philadelphia, PA 19112	1
Dr. Lionel Dickinson Naval Explosive Ordnance Disposal Tech. Center Code D Indian Head, MD 20640	1	Dr. H.G. Adolph Naval Surface Weapons Center Code R11 White Oak Silver Spring, MD 20910	1
Mr. C.L. Adams Naval Ordnance Station Code PM4 Indian Head, MD 20640	1	Dr. T.D. Austin Naval Surface Weapons Center Code R16 Indian Head, MD 20640	1
Mr. S. Mitchell Naval Ordnance Station Code 5253 Indian Head, MD 20640	1	Dr. T. Hall Code R-11 Naval Surface Weapons Center White Oak Laboratory Silver Spring, MD 20910	1
Dr. William Tolles Dean of Research Naval Postgraduate School Monterey, CA 93940	1	Mr. G.L. Mackenzie Naval Surface Weapons Center Code R101 Indian Head, MD 20640	1
Naval Research Lab. Code 6100 Washington, D.C. 20375	1	Dr. K.F. Mueller Naval Surface Weapons Center Code R11 White Oak Silver Spring, MD 20910	1

DISTRIBUTION LIST

	<u>No. Copies</u>		<u>No. Copies</u>
Mr. J. Murrin Naval Sea Systems Command Code 62R2 Washington, D.C. 20362	1	Dr. A. Nielsen Naval Weapons Center Code 385 China Lake, CA 93555	1
Dr. D.J. Pastine Naval Surface Weapons Center Code R04 White Oak Silver Spring, MD 20910	1	Dr. R. Reed, Jr. Naval Weapons Center Code 388 China Lake, CA 93555	1
Mr. L. Roslund Naval Surface Weapons Center Code R122 White Oak, Silver Spring MD 20910	1	Dr. L. Smith Naval Weapons Center Code 3205 China Lake, CA 93555	1
Mr. M. Stosz Naval Surface Weapons Center Code R121 White Oak Silver Spring, MD 20910	1	Dr. B. Douda Naval Weapons Support Center Code 5042 Crane, Indiana 47522	1
Dr. E. Zimmet Naval Surface Weapons Center Code R13 White Oak Silver Spring, MD 20910	1	Dr. A. Faulstich Chief of Naval Technology MAT Code 0716 Washington, D.C. 20360	1
Dr. D. R. Derr Naval Weapons Center Code 388 China Lake, CA 93555	1	LCDR J. Walker Chief of Naval Material Office of Naval Technology MAT, Code 0712 Washington, D.C. 20360	1
Mr. Lee N. Gilbert Naval Weapons Center Code 3205 China Lake, CA 93555	1	Mr. Joe McCartney Naval Ocean Systems Center San Diego, CA 92152	1
Dr. E. Martin Naval Weapons Center Code 3858 China Lake, CA 93555	1	Dr. S. Yamamoto Marine Sciences Division Naval Ocean Systems Center San Diego, CA 91232	1
Mr. R. McCarten Naval Weapons Center Code 3272 China Lake, CA 93555	1	Dr. G. Bosmajian Applied Chemistry Division Naval Ship Research & Development Center Annapolis, MD 21401	1
		Dr. H. Shuey Rohn and Haas Company Huntsville, Alabama 35801	1

DISTRIBUTION LIST

	<u>No. Copies</u>		<u>No. Copies</u>
Dr. J.F. Kincaid Strategic Systems Project Office Department of the Navy Room 901 Washington, D.C. 20376	1	Dr. C.W. Vriesen Thiokol Elkton Division P.O. Box 241 Elkton, MD 21921	1
Strategic Systems Project Office Propulsion Unit Code SP2731 Department of the Navy Washington, D.C. 20376	1	Dr. J.C. Hinshaw Thiokol Wasatch Division P.O. Box 524 Brigham City, Utah 84302	1
Mr. E.L. Throckmorton Strategic Systems Project Office Department of the Navy Room 1048 Washington, D.C. 20376	1	U.S. Army Research Office Chemical & Biological Sciences Division P.O. Box 12211 Research Triangle Park NC 27709	1
Dr. D.A. Flanigan Thiokol Huntsville Division Huntsville, Alabama 35807	1	Dr. R.F. Walker USA ARRADCOM DRDAR-LCE Dover, NJ 07801	1
Mr. G.F. Mangum Thiokol Corporation Huntsville Division Huntsville, Alabama 35807	1	Dr. T. Sinden Munitions Directorate Propellants and Explosives Defence Equipment Staff British Embassy 3100 Massachusetts Ave. Washington, D.C. 20008	1
Mr. E.S. Sutton Thiokol Corporation Elkton Division P.O. Box 241 Elkton, MD 21921	1	LTC B. Loving AFROL/LK Edwards AFB, CA 93523	1
Dr. G. Thompson Thiokol Wasatch Division MS 240 P.O. Box 524 Brigham City, UT 84302	1	Professor Alan N. Gent Institute of Polymer Science University of Akron Akron, OH 44325	1
Dr. T.F. Davidson Technical Director Thiokol Corporation Government Systems Group P.O. Box 9258 Ogden, Utah 84409	1	Mr. J. M. Frankle Army Ballistic Research Labs ARRADCOM Code DRDAR-BLI Aberdeen Proving Ground, MD 21005	1

DISTRIBUTION LIST

	<u>No. Copies</u>		<u>No. Copies</u>
Dr. Ingo W. May Army Ballistic Research Labs ARRADCOM Code DRDAR-BLI Aberdeen Proving Ground, MD 21005	1	Dr. J. P. Marshall Dept. 52-35, Bldg. 204/2 Lockheed Missile & Space Co. 3251 Hanover Street Palo Alto, CA 94304	1
Professor N.W. Tschoegl California Institute of Tech Dept. of Chemical Engineering Pasadena, CA 91125	1	Ms. Joan L. Janney Los Alamos National Lab Mail Stop 920 Los Alamos, NM 87545	1
Professor M.D. Nicol University of California Dept. of Chemistry 405 Hilgard Avenue Los Angeles, CA 90024	1	Dr. J. M. Walsh Los Alamos Scientific Lab Los Alamos, NM 87545	1
Professor A. G. Evans University of California Berkeley, CA 94720	1	Professor R. W. Armstrong Univ. of Maryland Department of Mechanical Eng. College Park, MD 20742	1
Professor T. Litovitz Catholic Univ. of America Physics Department 520 Michigan Ave., N.E. Washington, D.C. 20017	1	Prof. Richard A. Reinhardt Naval Postgraduate School Physics & Chemistry Dept. Monterey, CA 93940	1
Professor W. G. Knauss Graduate Aeronautical Lab California Institute of Tech. Pasadena, CA 91125	1	Dr. R. Bernecker Naval Surface Weapons Center Code R13 White Oak, Silver Spring, MD 20910	1
Professor Edward Price Georgia Institute of Tech. School of Aerospace Engin. Atlanta, Georgia 30332	1	Dr. M. J. Kamlet Naval Surface Weapons Center Code R11 White Oak, Silver Spring, MD 20910	1
Dr. Kenneth O. Hartman Hercules Aerospace Division Hercules Incorporated P.O. Box 210 Cumberland, MD 21502	1	Professor J. D. Achenbach Northwestern University Dept. of Civil Engineering Evanston, IL 60201	1
Dr. Thor L. Smith IBM Research Lab 042.282 San Jose, CA 95193	1	Dr. N. L. Basdekas Office of Naval Research Mechanics Program, Code 432 Arlington, VA 22217	1
		Professor Kenneth Kuo Pennsylvania State Univ. Dept. of Mechanical Engineering University Park, PA 16802	1

DISTRIBUTION LIST

	<u>No. Copies</u>	<u>No. Copies</u>
Dr. S. Sheffield Sandia Laboratories Division 2513 P.O. Box 5800 Albuquerque, NM 87185	1	
Dr. M. Farber Space Sciences, Inc. 135 Maple Avenue Monrovia, CA 91016	1	
Dr. Y. M. Gupta SRI International 333 Ravenswood Avenue Menlo Park, CA 94025	1	
Mr. M. Hill SRI International 333 Ravenswood Avenue Menlo Park, CA 94025	1	
Professor Richard A. Schapery Texas A&M Univ. Dept of Civil Engineering College Station, TX 77843	1	
Dr. Stephen Swanson Univ. of Utah Dept. of Mech. & Industrial Engineering MEB 3008 Salt Lake City, UT 84112	1	
Mr. J. D. Byrd Thiokol Corp. Huntsville Huntsville Div. Huntsville, AL 35807	1	
Professor G. D. Duvall Washington State University Dept. of Physics Pullman, WA 99163	1	
Prof. T. Dickinson Washington State University Dept. of Physics Pullman, WA 99163	1	

